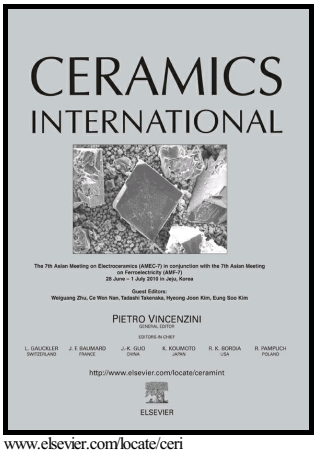


www.elsevier.com/locate/ceri

# 3D Characterization of Cubic Boron Nitride (CBN) Composites used as Tool Material for High Precision Abrasive Machining Processes

S. Fang, L. Llanes, D. Baehre, F. Muecklich

PII: S0272-8842(17)31646-2
DOI: http://dx.doi.org/10.1016/j.ceramint.2017.07.198
Reference: CERI15918

To appear in: *Ceramics International*

Received date: 13 July 2017
Revised date: 27 July 2017
Accepted date: 27 July 2017

Cite this article as: S. Fang, L. Llanes, D. Baehre and F. Muecklich, 3D Characterization of Cubic Boron Nitride (CBN) Composites used as Tool Material for High Precision Abrasive Machining Processes, *Ceramic International,* http://dx.doi.org/10.1016/j.ceramint.2017.07.198

# 3D Characterization of Cubic Boron Nitride (CBN) Composites used as Tool Material for High Precision Abrasive Machining Processes

S. Fang[a,b,c], L. Llanes[a,b], D. Baehre[c], F. Muecklich[d]

[a]CIEFMA-Departament de Ciència del Materials i Enginyeria Metal.lúrgica, Universitat Politècnica de Catalunya, EEBE - Campus Diagonal Besòs, 08019 Barcelona, Spain

[b]Barcelona Research Center in Multiscale Science and Engineering, Universitat Politècnica de Catalunya, 08019 Barcelona, Spain

[c]Institute of Production Engineering, Saarland University, 66123 Saarbrücken, Germany

[d]Institute of Functional Materials, Saarland University, 66123 Saarbrücken, Germany



**Abstract** Cubic boron nitride (CBN) composites are widely used as cutting tool materials for high precision abrasive machining processes. They are composed of super hard CBN abrasives and a softer binder. CBN abrasives are one of the hardest materials. They are embedded in the binder which can be metallic, polymeric or ceramic. The binder supports the abrasives and offers suitable toughness. The two components are consolidated by sintering processes under high pressure and temperature. Hence, abrasive particles exhibit an irregular spatial distribution in terms of size, location and orientation. In this work, X-ray computed tomography (CT scan) is used to investigate the geometrical properties of CBN abrasives in the volume regarding quantity, dimension and shape. A three-dimensional (3D) model is generated and the CBN abrasives are correspondingly characterized. The contribution includes both detailed explanation of CT scan and 3D modeling implementation, as well as quantification analysis of the key microstructural features for CBN composites.

Keywords: Cubic boron nitride; X-ray computed tomography; 3D modeling, quantification; characterization.

## 1. Introduction

Cubic boron nitride (CBN) is the second hardest substance after diamond [1]. Under high temperature and pressure, the structure of boron nitride is transformed from hexagonal to cubic [2]. Moreover, CBN exhibits not only better wear resistance, but also higher thermal conductivity than diamond. It implies a wider range of applications for CBN compared to diamond [1-3]. It is widely used as the hard phase within cutting tools for industrial abrasive machining processes, such as grinding and honing, and under harsh service conditions, i.e. elevated temperature or high speed [4,5]. CBN composites basically consist of two phases: CBN grains and a binder. According to its chemical nature, binder materials can be classified as metallic, polymeric (resin) and ceramic. CBN composites are sintered by mixing CBN particles and binder material powders under high temperature and vacuum. However, due to the manufacturing processes, the CBN particles are not regularly distributed in the produced composite. In addition, shape, dimension and orientation of the particles are not standardized.

During abrasive machining processes, the emerging CBN grains located on the cutting surfaces work as sharp edges and remove the material of workpiece. Therefore, geometrical properties of CBN grains can strongly influence the quality of the machined workpiece surfaces. For example, the produced surface roughness of the workpiece is, to some extent, determined by the protruding height of the grains [6]. Hence, the surface topography becomes relevant for correlating tool material characteristics and its performance. In a recent work by the authors, a two-dimensional (2D) quantification protocol has been proposed for assessing the geometrical properties of CBN grains on the cutting surfaces of a honing stone [7]. However, 2D characterization methods offer limited information related to three-dimensional (3D) subsurface features. This information may play an important role for understanding wear processes of the material, since the abrasive grains at the cutting surfaces are dynamically

changing during the machining processes due to a self-sharpening effect [8]. Therefore, it is relevant to extend the characterization and quantification of these composites, and particularly of the CBN grains, to a bulk-like (3D) perspective. It would enable to foresee the evolution of the cutting surfaces during the machining processes.

There are several advanced techniques to obtain a 3D volume reconstruction of microstructures and/or damage/cracking scenarios involved in materials science: electron tomography [9], atom probe tomography [10,11], focused ion beam tomography [12-15], and X-ray computed tomography [16,17], among others. Considering the length-scale of microstructural features exhibited by the CBN composites investigated, X-ray computed tomography (CT) emerges as the most appropriated technique for 3D microstructure characterization to be used in this study. It uses X-ray to produce 3D images of the scanned object [18,19]. Since its introduction in the 1970s, it has been mainly implemented in medicine as a remarkable development of the diagnosis method. The application of X-ray CT is now widely extended as it is also used in different industries (e.g. Refs. [20,21]). In the field of production engineering, X-ray CT is employed to inspect and characterize material deformation, internal flaws and crack propagation (e.g. Refs. [22,23]). Considering the subject of this paper, CT scan has been used to analyze the geometrical properties of single CBN grains, such as shape and dimension [24]. However, in order to quantitatively characterize CBN composites from a statistical point of view, it is necessary to obtain geometrical information of a large quantity of grains in a given (representative) volume. Within this context, the 3D volume quantification of CBN composites requires extensive data gathering and analysis together with effective modeling, so that the material volume may be reliably reconstructed. Under these conditions, the geometrical properties of a large number of grains could be statistically analyzed on the basis of their features, such as shape, dimension,

orientation and phase ratio. This is the main objective of the investigation presented in this paper.

## 2. Material, Data Analysis and Experimental Aspects

### 2.1 Investigated CBN Composite

The material studied in this paper is a commercial CBN honing stone which is referred to as B151/L2/10/50. The specification (Table 1) of this honing stone indicates the following data: the abrasive nature is Cubic Boron Nitride (B), the grain size is between 126 μm and 150 μm (151), a standard metallic (bronze-like nature) binder type of (L2) is used, the grain structure and quality (10) and grain concentration is 12.5 Vol-%, i.e. about 0.44 g/cm³ (50) [25,26]. Composite hardness ranges from 250 to 350 Vickers hardness (measured under applied load of 294N), in agreement with the relative amount of superhard phase embedded in a quite soft metallic matrix. Figure 1(a) shows the surface image of CBN composite obtained by scanning electron microscopy, and Figure 1(b) shows the 3D image of a CBN grain obtained by laser scanning microscopy.

### 2.2 Software Programs for Image Processing and Quantitative Analysis of Microstructures

Two software programs are used in the study: 3D modeling and processing software AMIRA 5 (FEI Company) and MAVI (Fraunhofer Institute for Industrial Mathematics). AMIRA 5 is a competent software tool for 3D image processing. It can visualize raw data (2D images) obtained from microscopy or tomography, manipulate and enhance image processing and reconstruct the studied volume by assembling cross-sectional 2D images. MAVI is employed

as an additional unit to complement volume image analysis after the bulk reconstruction. It permits to carry out quantitative analysis of the studied microstructures.

2.3 3D Volume Quantification Parameters

The main objective of the investigation is to propose a method to quantify and analyze grain geometrical properties of the honing stone B151 with a 3D statistical perspective. During the investigation procedure, the volume of the studied material is reconstructed with a series of binarized cross-sectional images obtained by the CT-scan. Based on the reconstructed volume, key geometrical properties of the grains in the investigated volume, such as quantity, dimension and form (Figure 2) are assessed.

Quantity Parameters

Four parameters (Table 2) are used to describe the quantity features: grain amount $N_t$, grain volume fraction $f_g$, binder volume fraction $f_b$ and particle density D. Grain/binder volume fraction $f_g/f_b$ is calculated by equation (1):

$$f_g = \frac{V_g}{V_s} \text{ or } f_b = \frac{V_b}{V_s} \quad (1)$$

where

$V_g$: total grain volume

$V_b$: total binder volume

$V_s$: total specimen volume

On the other hand, particle density $D$ is calculated by equation (2):

$$D = \frac{N_t}{V_s} \quad (2)$$

where

$N_t$: Grain amount

Dimensional Parameters

Three parameters (Table 3) are employed to assess the dimensional features of the grains: mean grain surface $\bar{S}_g$, mean grain volume $\bar{V}_g$ and equivalent spherical diameter $D_{eq}$.

Form Parameters

Three isoperimetric shape factors are introduced to describe the shape of the intrinsic volumes of convex and compact grains with non-empty interior [27]. For each grain, three shape factors are calculated – by equation (3) – using parameters *V*, *S* and *M* which represent volume, surface area and integral of mean curvature of grains, respectively. *M* is given by equation (4) where $1/r_1(s)$ and $1/r_2(s)$ are the minimum and maximum curvature at the surface element *ds*, and $\partial b$ is the boundary of the grain [28]. The values of the three parameters are obtained by the grain quantification.

$$f_1 = 6\sqrt{\pi}\frac{V}{\sqrt{S^3}}$$

$$f_2 = 48\pi^2\frac{V}{M^3}$$

$$f_3 = 4\pi\frac{S}{M^2} \tag{3}$$

$$M = \int_{\partial b}\frac{1}{2}\left(\frac{1}{r_1(s)} + \frac{1}{r_2(s)}\right)\mathrm{ds} \tag{4}$$

Meanwhile, the grains can be classified using three corresponding geometrical features, i.e. length, width and thickness of the grain. Three basic shapes (Figure 3 (a)) are defined according to correlations among these three features [29]:

- granule, when length, width and thickness are approximately equal;
- chip, when length and width are approximately equal, but different from thickness, or the three parameters are different from each other;
- fiber, when width and thickness are approximately equal, but different from length.

Taking into consideration the calculated values of the three isoperimetric shape factors, grains can be classified into three basic shape categories (Figure 3(b)) [30]:

- when $f_3 \leq 0.5$ and $f_2 \leq 0.1$, it is a fiber;
- if it is not a fiber, and when $f_1 \leq 0.7$ and $f_2 \leq 0.4$, then it is a chip;
- if it is neither fiber nor a chip, then it is a granule.

2.3 Experimental Procedure

The procedure of 3D volume quantification is shown in Figure 4, including three steps: image acquisition, segmentation and image processing, and finally 3D modeling and quantification [31].

Image Acquisition

A specimen of the honing stone B151/L2/10/50 (B151) with a volume of 2844 μm×16980 μm ×1765 μm has been scanned via CT scan in order to acquire cross-sectional 2D images. As it is shown in figure 5, the sample is fixed on the holder between the X-ray illuminator and detector. When the illuminated X-ray passes through the sample, it is either absorbed or scattered. Hence, a “shadow” is projected on the X-Ray detector. As CBN grains in the

specimen do not have identical geometry features, and as they are also randomly distributed and oriented, the projected shadows have different intensities. The shadow intensity which is measured and recorded by the detector as a 2D image, contains the density of the investigated material and the geometrical information of the CBN grains. As the holder can rotate 360°, it permits to investigate the whole volume from each direction. With a special agglomeration, a series of 2D images from various layers of the CBN specimen is then obtained by the CT scan. The series obtained by the CT scan includes 130 images on the XY-plane with the thickness of 13.6 µm along the Z-axis. The images have the size of 241 pixels along the X-axis and 1439 pixels along the Y-axis. Therefore, the pixel size is 11.8 µm along both X- and Y-axis, and 13.6 µm along the Z-axis, taking into account that the cross-sectional image has the size of 2844 µm×16980 µm on the XY-plane. The calculated voxel size is 1.9 $x10^3$ $\mu m^3$. Figure 6 shows the cross-sectional scanning and a cross-sectional image of the CBN composite on the XY-plane, as obtained by the CT scan.

Segmentation and Image Processing

In this step, the images are treated in order to obtain binary images with white background and black blocks. The white background and black blocks represent the binder and the grains of the CBN honing stone, respectively. This step is essential for this investigation since the reliability of 3D grain quantification is based on the geometrical properties of the extracted black blocks, such as number, size and form. However, it is noticeable that the original images obtained by the CT scan are not well contrasted in some parts, i.e. the separation between the bright phase and the dark one is not clear. These are some common defaults induced during the image acquisition step, such as lack of contrast, grain adhesion and blur edge (Figure 7). Taking into account that the main goal of this step is to determine the clear border between the grain and the binder, the aforementioned defaults should then be corrected by morphological treatments. These were carried out by means of the series of algorithm

operations: Filter Alignment, Filter Global Thresholding, Filter Resampling Low Pass and Filter Edge-Preserving Smoothing. These algorithm operations can be employed in conjunction with each other or individually, according to the correlation of position, contrast and smoothness.

The operation Filter Alignment is applied to adjust the position of each image along the cross-section direction in the image acquisition, preventing the shift of image assemblage in the 3D volume reconstruction. In this case, the obtained images should be adjusted on the XY-plane perpendicular to the Z-axis (Figure 6(a)). This operation is mandatory if the cross-sectioning is done manually, e.g. by means of polishing. The greyscale images obtained by the CT scan are composed of pixels. The pixel represents the smallest constituent element of a digital image. In a greyscale image, each pixel is encoded on a fixed value from 0 to 255 (grey scale). Conventionally, 0 is the darkest value (black) and 255 is the brightest one (white). Hence, if the encoded pixels of an image possess high grey values (towards 255), the image appears bright. On the contrary, it appears dark. The operation Filter Global Thresholding is employed to roughly select the black blocks out of the grey field, and to determine their borders by setting a range of grey values for each pixel. The operation Filter Global Thresholding can be described as follows:



If $\mathbf{I_{i,j}} \leq \mathbf{T_{inf}}$ **,** then $\mathbf{I_{i,j}} = \mathbf{0}$ (white)

If $\mathbf{I_{i,j}} \geq \mathbf{T_{sup}}$, then $\mathbf{I_{i,j}} = \mathbf{255}$ (black)

where

$\mathbf{I_{i,j}}$: grey value of a pixel with spatial coordinate **i,j**,

$\mathbf{T_{inf}}$ and $\mathbf{T_{sup}}$: inferior and superior fixed Thresholding grey values, respectively.

In this case, the inferior value is set to be 105 and the superior one to be 126. After the application of the operation Filter Global Thresholding, all pixels below and equal to $\mathbf{T_{inf}}$= 105 take the grey value of 0. On the other hand, all pixels above and equal to $\mathbf{T_{sup}}$= 126 take the grey value of 255. Compared with the original grey scale image obtained by the CT scan (Figure 8(a)), most of the grains are extracted from the grey field and given a defined border (Figure 8(b)). However, it is noticeable that the extracted grains exhibit different brightness gradients at their borders due to variant pixel values between 105 and 126. Next, the operation Filter Resampling Low Pass is performed to sharpen the borders and make them appear sufficiently pronounced. The function calculates the intermediate grey value, i.e. 115 in this case. The pixels at the border are given the grey value of 0 (black) if their initial grey values are inferior to 115. Otherwise, they are given the value of 255 (white) (Figure 9(a)). Therefore, a binary image encoded on 0 (black, grains) and 255 (white, binder) is then obtained (Figure 8(c)). After this step, the operation Filter Edge-Preserving Smoothing is necessary to reduce the noise and smooth the grain borders (Figure 8(d)). In this operation, the grey value of each pixel at grain border is attributed the median value of their neighboring pixels. The median value is calculated by first sorting all the pixel values from the surrounding neighborhood into numerical order with a range of N*N neighboring pixels. Then the considered pixel is replaced by the median pixel value. In Figure 9(b), for example, the highlighted pixel on the border before the application of the filter has a value of 2, corresponding to white. Its neighboring pixels in a 5*5 matrix with the values 1 and 2, corresponding to black and white, have the values in numerical order: 1;1;1:1;1;1;1;1;1;1;1;1;1;1;2;2;2;2;2;2;2;2;2;2;2. The median value is then the $13^{th}$ one, i.e. 1, which corresponds to black. Hence, the value of the highlighted pixel is then set to be 1 after the application of Filter Edge-Preserving Smoothing. The color is then changed to black and the border becomes smooth.

Final 3D Modeling and Quantification

Based on the Image Processing and Segmentation step, the grains are separated from the binder and a binary grey value is then assigned to each grain. In this final step, the scanned volume is then reconstructed using the software AMIRA 5. Important geometrical and microstructural parameters are quantified using the aforementioned algorithms by the software MAVI [28,32,33].

## 3. Results and Discussion

### 3.1 3D Volume Reconstruction and Microstructural Information

The grains in the investigated volume after the segmentation are visualized in Figure 10. Shapes of grain cross-sections are not identical, but most of them are polygons according to the cross-sectional image (Figure 10(a)). It is noticeable that the grain shapes vary and that they are oriented differently. Figure 10(b) shows that the grains are also randomly distributed in the volume.

### 3.2 Quantity Parameters

Table 4 presents the statistical results of the microstructural information of the reconstructed 3D model. It has been found that there are 4093 CBN grains in the volume $V_s$ of $8.5\times10^{10}$ µm³. Hence, the grain density is 48 grains/mm³. In the reconstructed specimen volume, all the grains have the volume $V_g$ of $0.7\times10^{10}$ µm³, whereas the binder has the volume $V_b$ of $7.8\times10^{10}$ µm³. Therefore, grains and binder account for 8.2% and 91.8%, respectively, of the entire volume.

### 3.3 Dimensional Parameters

Table 5 shows the dimensional properties of the B151 grains in the reconstructed volume. Mean grain volume $\bar{V}_g$ and mean grain surface $\bar{S}_g$ are $1.6\times10^6$ µm³ and $7.7\times10^4$ µm², respectively. Considering that grains are spheres, the equivalent diameter $D_{eq}$ is then calculated to be 132 µm, which is slightly deviatied from the nominal mean grain size, i.e. 138 µm (Table 1).

Figure 11(a) shows the distribution of the grain amount as a function of the equivalent spherical diameter of grains $D_{eq}$. The distribution of the grain amount is close to a Gaussian approximation, where most of the grains are distributed near the mean equivalent spherical diameter of grains $D_{eq}$, i.e. 132 µm. It is found that about 250 grains exhibit a $D_{eq}$ lower than 30 µm, which accounts for only 0.02% volume of all the grains. These 250 grains are considered as induced defaults during the imaging processing, where some individual small particles are produced due to the separation of big ones. Some extreme coarse grains (larger than 240 µm) have also been found due to the modeling error. On the other hand, some contacting grains have been considered as one large grain by the software, and were therefore not separated in the image processing. Figure 11(b) shows the volume fraction as a function of the equivalent spherical diameter. The distribution has also a Gaussian approximation and is similar to the distribution of the grain amount.



3.4 Form Parameters

When the pixel amount of a particle is too small, the calculation of its shape factors becomes impossible, since the software requires the particle to have at least two pixels along each axis (i.e. 8 voxels) to obtain reliable shape factors. In this case, the grain should have a diameter larger than 30 µm (approximately corresponding with the volume of 8 voxels, i.e. 1.5 x$10^4$ µm³). Otherwise, the shape classification is not reliable anymore. Therefore, about 250 grains with diameters lower than 30 µm should be eliminated in order to analyze the grain shape.

Then, namely 3843 grains have been analyzed. According to the aforementioned dimensional analysis of the grains, the tiny ones (with a diameter lower than 30µm) are considered as introduced defaults, since such tiny grains should not exist in the honing stone B151. Table 6 shows the grain shape classification. It is roughly found that 31 grains are fibers, 748 grains are chips and 3064 grains are granules. Hence, fibers account for 0.8%, chips for 19.5% and granules for 79.7% of all the grains.

## 4. Summary and Concluding Remarks

In this investigation, the 3D volume quantification of a commercial CBN honing stone B151 has been conducted, based on 3D modeling and volume reconstruction. A CT scan has been employed to acquire series of cross-sectional images of the investigated volume with a high resolution. Image processing software Amira and MAVI were applied to reconstruct the volume and to quantify the grains in terms of quantity, dimension and form.

Compared to the traditional two-dimensional (2D) surface quantification method, the investigation scale in the 3D quantification is extended from surface to volume. Then, a larger quantity of CBN grains in the honing stone B151 is involved in the investigation and more satisfactory and reliable results are obtained from a statistical point of view. For instance, the obtained mean grain size of $D_{eq}$ is 132 µm in the 3D volume quantification, which is much closer to the nominal one of 138 µm compared to that of 123 µm obtained in the 2D surface quantification [7].

Furthermore, due to the utilization of the CT scan, the 3D volume quantification is a non-destructive method without physical contact. Hence, the requirement of sample geometry

becomes less important compared to other image acquisition methods, such as polishing-microcopy or FIB cross-section. It is also more adaptable to study the samples with more complex shape. It may also avoid metallographic preparation which in certain cases can induce unexpected defaults and have negative influence on the image acquisition outcomes. These advantages are relevant compared not only to the 2D surface quantification method, but also to some other 3D investigation methods, e.g. FIB cross-section, for which a flat and polished surface is usually necessary for image acquisition and the bulk amount being characterized is significantly smaller.

As a final remark, it may be stated that 3D volume quantification is an effective characterization technique for CBN composites. In general, it can be pointed out not only for assessment of microstructural properties, but also as a technique that could be adapted for quality inspection of material fabrication or tool performance prediction.



**Acknowledgements**

The work leading to this publication was supported by the German Academic Exchange Service (DAAD) with funds from the German Federal Ministry of Education and Research (BMBF) and the People Program (Marie Curie Actions) of the European Union's Seventh Framework Program (FP7/2007-2013) under REA grant agreement n° 605728 (P.R.I.M.E. – Postdoctoral Researchers International Mobility Experience). The authors are also grateful for equipment support from Fraunhofer Institute for Non-destructive Testing IZFP, as well as for the material supplying by KADIA Produktion GmbH + Co. Finally, this contribution has also been partly funded by the Spanish Ministry of Economy and Competitiveness through Grant MAT2015-70780-C4-3P (MINECO/FEDER).

**References**

[1] S. N. Monteiro, A. L. D. Skury, M. G. de Azevedo, G. S. Bobrovnitchii, "Cubic boron nitride competing with diamond as a superhard engineering material – an overview," *J. Mater. Res. Technol.* 2 (2013) 68–74.

[2] R. H. Wentorf Jr., "Synthesis of the cubic form of boron nitride," *J. Chem. Phys.* 34 (1961) 809-812.

[3] P. Loginov, L. Mishnaevsky Jr., E. Levashov, M. Petrzhik, "Diamond and cBN hybrid and nanomodified cutting tools with enhanced performance: Development, testing and modelling", *Mater. Design* 88 (2015) 310–319.

[4] S. Saketi, S. Sveen, S. Gunnarsson, R. M'Saoubi, M. Olsson, "Wear of a high cBN content PCBN cutting tool during hard milling of powder metallurgy cold work tool steels," *Wear* 332–333 (2015) 752–761.

[5] Y. Wang, K. Lei, Y. Ruan, W. Dong, "Microstructure and wear resistance of c-BN/Ni–Cr–Ti composites prepared by spark plasma sintering," *Int. J. Refract. Met. Hard Mater.* 54 (2016) 98–103.

[6] L. Sabri, L., S. Mezghani, M. El Mansori, "A study on the influence of bond material on honing engine cylinder bores with coated diamond stones", *Surf. Coat. Technol.* 205 (2010) 1515-1519.

[7] S. Fang, L. Llanes, M. Engstler, D. Baehre, F. Soldera, F. Muecklich, "Surface topography quantification of super hard abrasive tools by laser scanning microscopy," *Mater. Perform. Charact.* 5 (2016) 1–20.

[8] F. Klocke, W. König, Fertigungsverfahren 2: Schleifen, Honen, Läppen (Manufacturing processes 2: grinding, honing, lapping), Springer-Verlag, Berlin and Heidelberg, Germany (2005) pp. 251-257.

[9] M. Hayashida, M. Malac, "Practical electron tomography guide: Recent progress and future opportunities," *Micron* 91 (2016) 49-74.

[10] E.A. Marquis, M. Bachhav, Y. Chen, Y. Dong, L.M. Gordon, A. McFarland, "On the current role of atom probe tomography in materials characterization and materials science," *Current Opinion in Solid State and Materials Science* 17 (2013) 217-223.

[11] D. Beinke, C. Oberdorfer, G. Schmitz, "Towards an accurate volume reconstruction in atom probe tomography," *Ultramicroscopy* 165 (2016) 34-41.

[12] J.M. Tarragó, G. Fargas, L. Isern, S. Dorvlo, E. Tarrés, C.M. Müller, E. Jiménez-Piqué, L. Llanes, "Microstructural influence on tolerance to corrosion-induced damage in hardmetals," *Mater. Design* 111 (2016) 36-43.

[13] C.R. Mayer, J. Molina-Aladareguia, N. Chawla, "Three dimensional (3D) microstructure-based finite element modeling of Al-SiC nanolaminates using focused ion beam (FIB) tomography," *Mater. Charact.* 120 (2016) 369-376.

[14] A.J. Gant, J.W. Nunn. M.G. Gee, D. Gorman, D.D. Gohil, L.P. Orkney, "New perspectives in hardmetal abrasion simulation," *Wear* 376-377 (2017) 2-14.

[15] E. Jiménez-Piqué, M. Turon-Vinas, H. Chen, T. Trifonov, J. Fair, E. Tarrés, L. Llanes, "Focused ion beam tomography of WC-Co cemented carbides," *Int. J. Refract. Met. Hard Mater.* 67 (2017) 9-17.

[16] l. Salvo, M. Suéry, A. Marmottant, N. Limodin, D. Bernard, "Imaging in material science: Application of X-ray tomography," C. R. Physique 11 (2010) 641-649.

[17] X. Gao, X. Han, Y. Song, "X-ray computed tomography based microstructure reconstruction and numerical estimation of thermal conductivity of 2.5D ceramic matrix composite," Ceram. Int. 43 (2017) 9790-9797.

[18] G. N. Hounsfield, "Computed medical imaging," *Science* 210 (1980) 22-28.

[19] J. Husband, G. Dombrowe, "X-ray computed tomography - a truly remarkable medical development," *Br. J. Radiol.* 78 (2005) 97–98.

[20] M. Bieberle, F. Barthel, U. Hampel, "Ultrafast X-ray computed tomography for the analysis of gas–solid fluidized beds," Chem. Eng. J. 189–190 (2012) 356-363.

[21] J.P. Mathews, Q.P. Campbell, H. Xu, P. Halleck, "A review of the application of X-ray computed tomography to the study of coal," *Fuel* 209 (2017) 10-24.

[22] J. Marrow, C. Reinhard, Y. Vertyagina, L. Saucedo-Mora, D. Collins, M. Mostafavi, "3D studies of damage by combined X-ray tomography and digital volume correlation," *Proc. Mater. Sci.* 3 (2014) 1554–1559.

[23] P. J. Liotier, V. Alain, D. Christine, "Characterization of 3D morphology and microcracks in composites reinforced by multi-axial multi-ply stitched preforms," *Compos. Part A Appl. Sci. Manuf.* 41 (2010) 653–662.

[24] K. Brakhage, M. Makowski, F. Klocke, M. Weiss, "Grinding wheel modeling: Development of a mathematical model," MASCOT11 Proceedings—IMACS Ser Comput Appl Math, 2011.

[25] F. Gerhard, Grundlagen und Anwendungen des Honens (Fundamentals and applications of honing), Vulkan-Verl., Essen, Germany, (1992) p.73.

[26] F. Klocke, W. König, Fertigungsverfahren 2: Schleifen, Honen, Läppen (Manufacturing processes 2: grinding, honing, lapping), Springer-Verlag, Berlin and Heidelberg, Germany, pp. 58-60, 2005.

[27] D. Stoyan, W. S. Kendall, J. Mecke, Stochastic geometry and its applications. J. Wiley & Sons, Chichester, New York, (1995) p. 436.

[28] J. Ohser, F. Mücklich, Statistical analysis of microstructures in materials science, John Willey & Sons, Chichester, New York (2000).

[29] T. Zingg, "Beitrag zur Schotteranalyse (Contribution to the gravel analysis)," *Schweizerische Miner ogische Petrogr Mitteilungen* 15 (1935) 39–140.

[30] I. Vecchio, K. Schladitz, M. Godehardt, M. J. Heneka, "3D geometric characterization of particles applied to technical cleanliness," *Image Anal. Stereol.* 31 (2012) 163–174.

[31] A. Velichko, M. Engstler, C. Selzner, F. Mücklich, "3D quantitative characterization of local structure and properties of contact materials," *Mater. Res. Soc. Symp. Proc.* 1184 (2009) 145–150.

[32] J. Ohser, W. Nagel, K. Schladitz, "The euler number of discretised sets – surprising results in three dimensions," *Image Anal. Stereol.* 22 (2011) 11-19.

[33] A. Velichko, C. Holzapfel, A. Siefers, K. Schladitz, F. Mücklich, "Unambiguous classification of complex microstructures by their three-dimensional parameters applied to graphite in cast iron," *Acta Mater.* 56 (2008) 1981–1990.

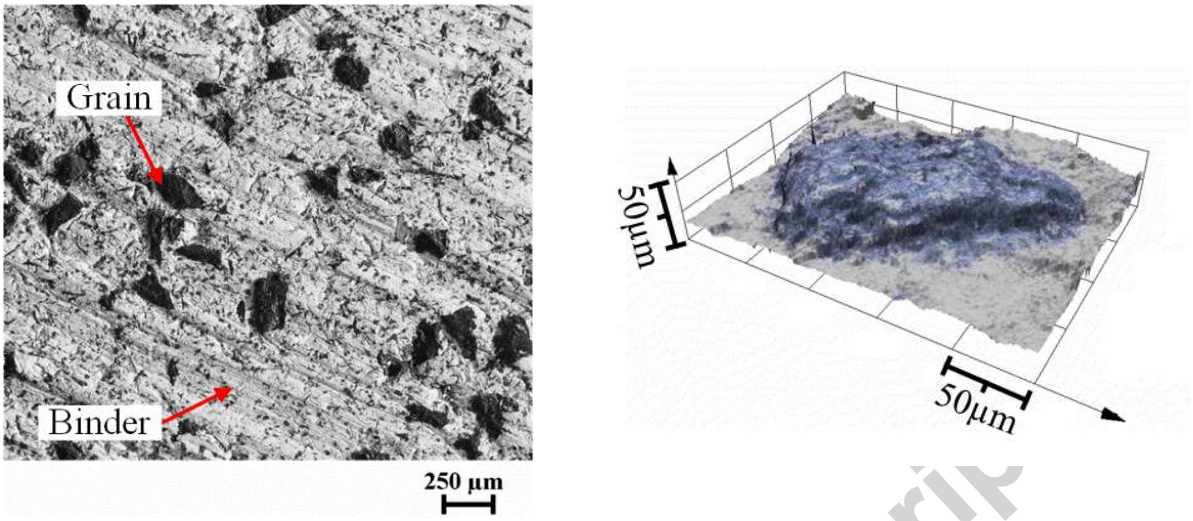


(a) (b)

Figure 1. (a) CBN composite surface image obtained by SEM, (b) CBN grain 3D image obtained by LSM.

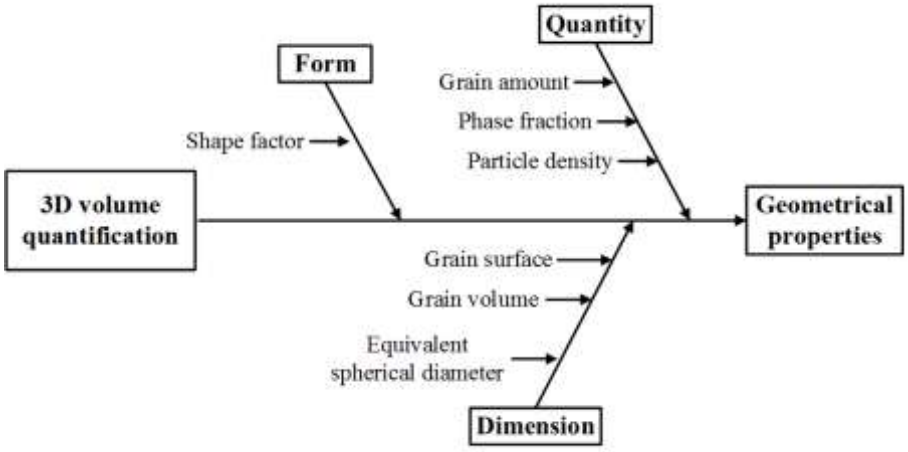


Figure 2. Assessment parameters of the 3D volume quantification of CBN honing stone B151.

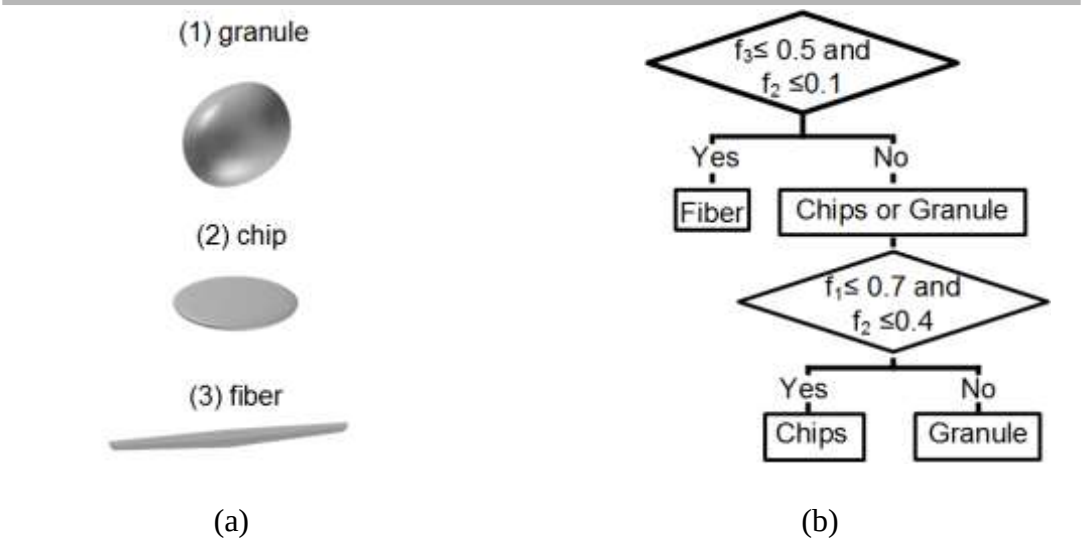


(a) (b)

Figure 3. (a) Basic grain shape definitions, (b) grain shape classification using shape factors.

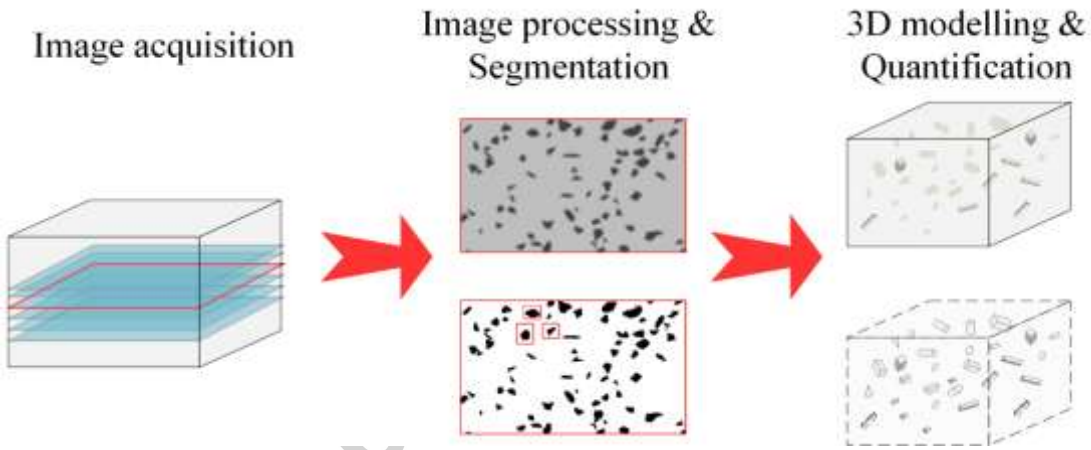


Figure 4. Procedure of volume reconstruction and 3D characterization.

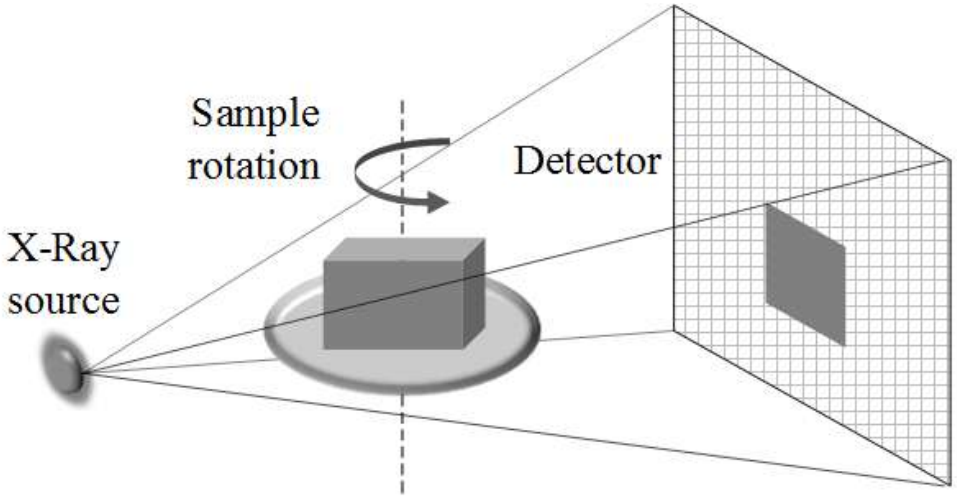


Figure 5. Schematic illustration of image acquisition using CT scan.

(a)

(b)

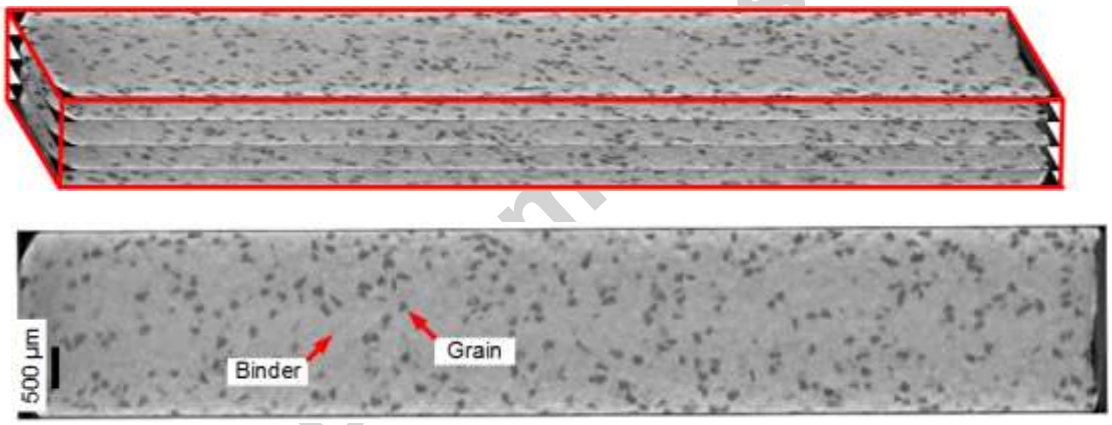


Figure 6. B151 (a) Cross-sectional scanning and (b) cross-sectional image of CBN composite obtained by CT scan.

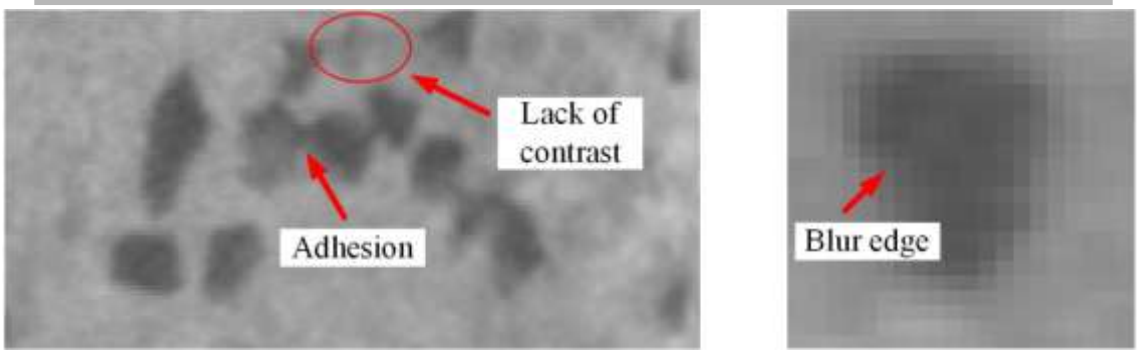


Figure 7. Common defaults induced in the image acquisition by the CT scan.

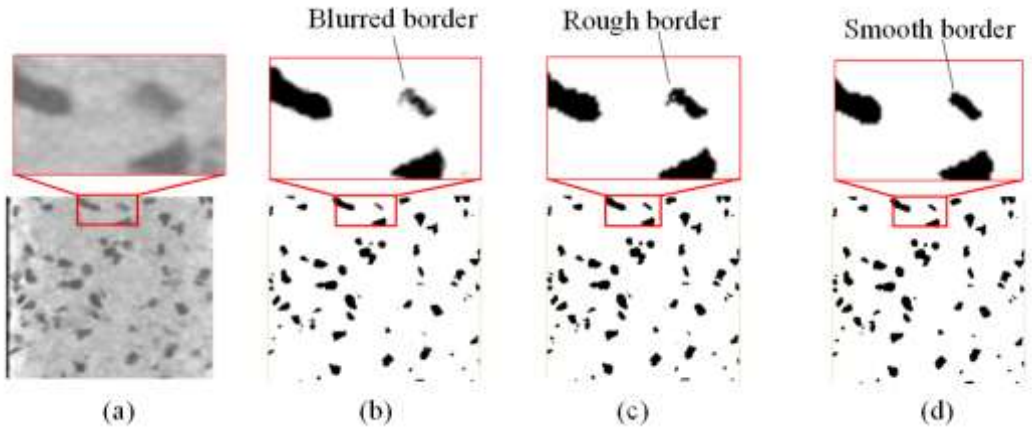


Figure 8. Morphological treatment of the acquired images: (a) original image without treatment, (b) filter Global Thresholding, (c) filter Resampling Low Pass, (d) filter Edge-Preserving Smoothing.

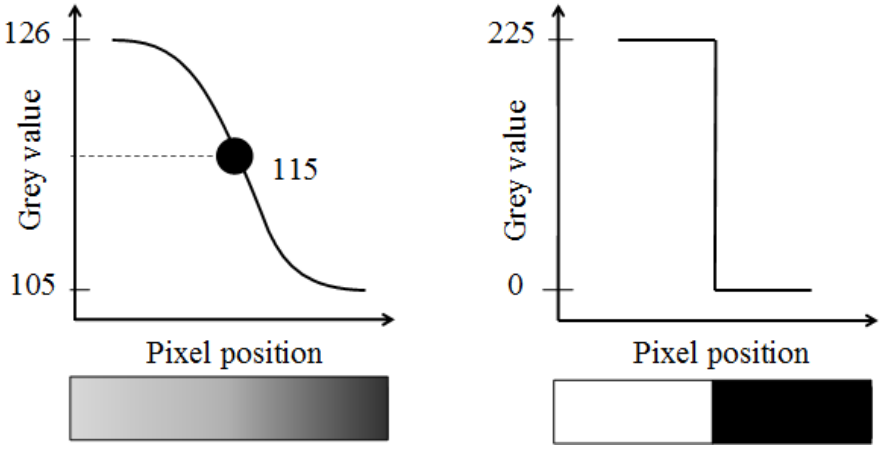


(a)

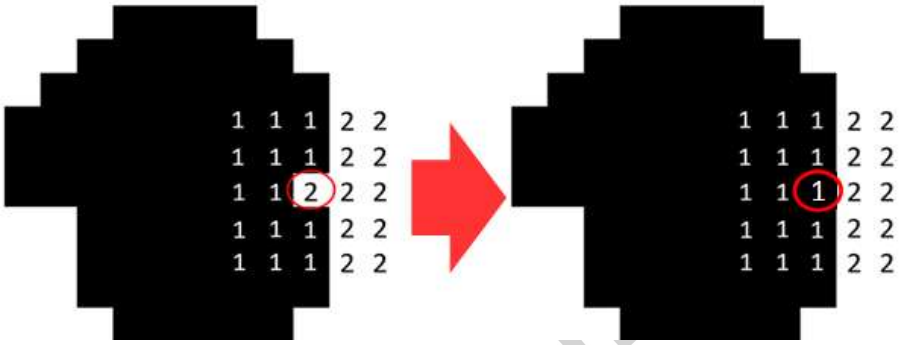


(b)

Figure 9. Graphical illustration of the agglomerations: (a) Filter Resampling Low Pass, (b) Filter Edge-Preserving Smoothing.

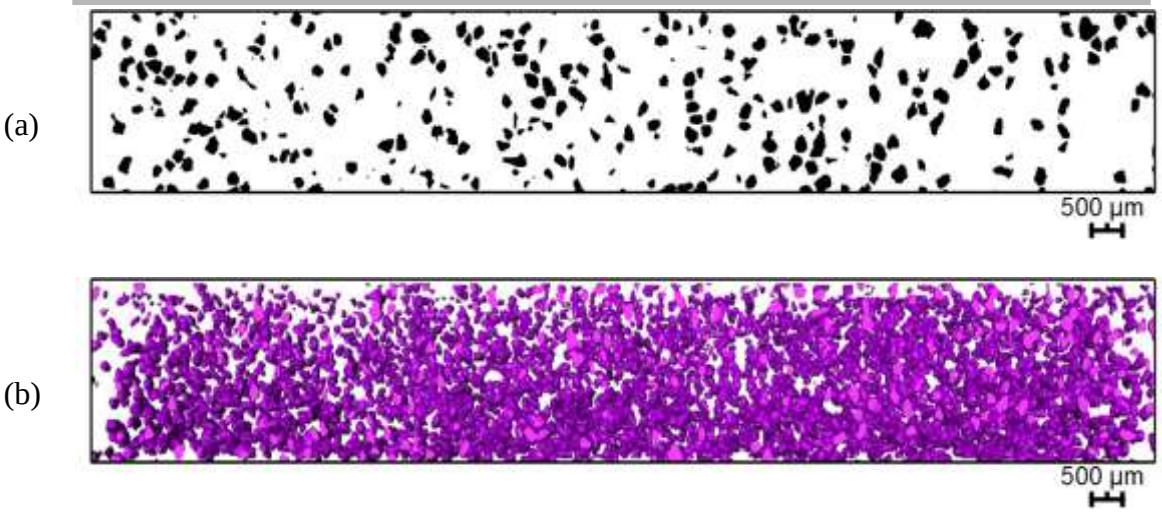


Figure 10. Grain segmentation of the specimen: (a) segmented cross-section image of the reconstructed 3D model, (b) grain distribution in the 3D model.

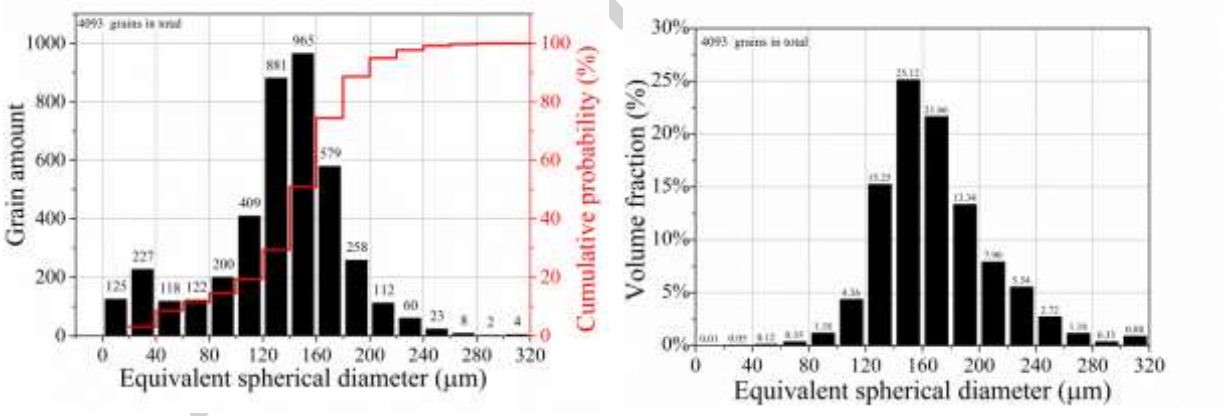


(a) (b)

Figure 11. (a) Distribution of the grain amount and (b) volume fraction distribution as a function of equivalent spherical diameter.

Table 1. Properties of the honing stones B151/L2/10/50.

| Honing Stone | Mean grain size (µm) | Max. grain size (µm) | Min. grain size (µm) | Grain concentration (Vol-%) | Density(g/cm³) |
|---|---|---|---|---|---|
| B151 | 138 | 150 | 126 | 12.5 | 0.44 |

Table 2. List of quantity parameters.

| Parameter | Definition |
|---|---|
| Grain amount $N_t$ | number of all the observed grains in the investigated volume |
| Grain volume fraction $f_g$ | ratio of the total grain volume ($V_g$) to the total specimen volume ($V_s$) |
| Binder volume fraction $f_b$ | ratio of the total binder volume ($V_b$) to the total specimen volume ($V_s$) |
| Particle density $D$ | grain amount per $mm^3$ |

Table 3. List of dimensional parameters.

| Parameter | Definition |
|---|---|
| Mean grain surface $\bar{S}_g$ | average value of grain surface area |
| Mean grain volume $\bar{V}_g$ | average value of grain volume |
| Equivalent spherical diameter $D_{eq}$ | average value of diameters of the equivalent spheres, which have identical volumes of the investigated grains |

Table 4. Microstructural information of the B151 specimen.

| Grain quantity | Grain density ($mm^{-3}$) | Specimen volume $V_s$ ($x10^{10}$ µm³) | Total grain volume $V_g$ ($x10^{10}$ µm³) | Total binder volume $V_b$ ($x10^{10}$ µm³) | Grain volume fraction $f_g$ (%) | Binder volume fraction $f_b$ (%) |
|---|---|---|---|---|---|---|
| 4093 | 48 | 8.5 | 0.7 | 7.8 | 8.2 | 91.8 |

Table 5. Dimensional properties of the B151 grains.

| Mean grain volume $\bar{V}_g$ ($\times 10^6$ µm³) | Mean grain surface $\bar{S}_g$ ($\times 10^4$ µm²) | Equivalent spherical diameter of grains $D_{eq}$ (µm) |
|---|---|---|
| 1.6 | 7.7 | 132 |

Table 6. Grain shape classification of the B151 specimen.

| Shape | Quantity | Fraction (%) |
|---|---|---|
| Granule | 3064 | 79.7 |
| Chip | 748 | 19.5 |
| Fiber | 31 | 0.8 |